In: AIAA SCITECH 2024 Forum, 8-12 January 2024, Orlando, USA, Paper number AIAA 2024-2854
DOI: 10.2514/6.2024-2854

Aerodynamics Analysis of Saab 340B Aircraft with Data Fusion Implementation

Kadir E. SAHIN[1], Fazil S. Gomec[2], Murat MILLIDERE[3] and James F. WHIDBORNE[4]
Cranfield University, College Rd, Wharley End, Bedford MK43 0AL
Turkish Aerospace, Ankara, Turkey

This paper conducts an aerodynamic analysis of the Saab 340B passenger aircraft, employing AVL and as numerical methods and DATCOM as a collection of engineering methods and empirical data that provide a set of aerodynamic coefficients for assessment. The investigation is focused on examining the longitudinal aerodynamic behavior of aircraft, specifically considering the impacts of flaps and elevators at varying angles of attack. The outcomes from the clean configuration are compared with the results obtained from computational fluid dynamics studies found in existing literature. While the results may not precisely match, they capture the general trends in the behavior of the aircraft. This aligns with the expected outcomes from preliminary methods like AVL and DATCOM. Data fusion techniques are strategically employed to integrate insights from these diverse sources, enhancing the overall accuracy and reliability of the aerodynamic assessment. The research aims to provide a comprehensive understanding of the clean configuration's aerodynamic performance, contributing significantly to the advancement of aviation technology.

Nomenclature

AVL = Athena Vortex Lattice
DATCOM= Digital DATa COMpendium
HF = High-Fidelity
LF = Low-Fidelity
MF = Multi-Fidelity
DOE = Design of Experiment
C_L = Lift Force Coefficient
C_D = Drag Force Coefficient
C_m = Pitching Moment Coefficient
α = Angle of Attack
δ_e = Horizontal Tail Deflection
δ_{lef} = Flap Deflection
GA = Genetic Algorithm
z = Observed Response Data
y = Model Response Data
n = Number of samples in the Dataset
cor = Correlation of Dataset
CFD = Computational Fluid Dynamics
VCM = Variable Complexity Modelling
MSE = Mean Square Error
RMSE = Root Mean Square Error
R2 = The Coefficient of Determination
ANN = Artificial Neural Network
FNN = Feedforward Neural Network
MLP = Multi-Layer Perceptron
DNN = Deep Neural Network
GA = Genetic Algorithm
DNGN = Deep Neural-Genetic Network
SFDNGN = Single-Fidelity Deep Neural-Genetic Network
MFDNGN = Multi-Fidelity Deep Neural-Genetic Network

[1]Graduate MSc Student, Centre of …, Cranfield University
[2]Aeroacustic Lead Engineer, Turkish Fighter Aircraft Division, Turkish Aerospace
[3]Research Fellow, Centre of Aeronautics, SATM, Cranfield University, AIAA Member.
[4]Prof, Centre of Aeronautics, SATM, Cranfield University.

I.Introduction

Aerodynamics analysis of passenger aircraft involves studying how air influences its performance and behavior throughout flight. This includes understanding how the wings generate lift to keep the aircraft in the air, managing drag for fuel efficiency, and examining stability and control features. Researchers use tools like wind tunnel testing and computational simulations to assess the impact of different configurations, control surfaces, and high-lift devices. The goal is to optimize the aircraft's design to ensure safe and efficient operation across various flight conditions, from takeoff to landing. In addition, Aircraft flight simulation is a key component of modern aircraft design, certification process and aircraft pilots training and the aerodynamic model is the core of a flight simulator. An error in the aerodynamic model can lead to a simulation which might fail in the qualification process.

To anticipate the possible fatal errors before actual flight tests and qualification process, aerodynamic analysis, and generation of aerodynamics dataset for aircraft play crucial role. These processes are essential for creating reliable dynamic flight simulations preventing waste of resources and improving aircraft safety and performance. There are several methods to generate aerodynamic dataset. These are semi-empirical methods, linear flow solvers, nonlinear flow solvers, small scale wind tunnel tests, full scale wind tunnel tests and flight tests in the increasing order of fidelity. As fidelity increases, processing time and cost increase. For aerodynamic database generation, various computational and experimental methods can be utilized with respect to the cost and accuracy requirements of the design phase. A summary of these methods with sample tools and classifications are provided in [1] [2].

As expected, the higher the cost, the more accurate the aerodynamic database. The resource and time cost of each method are essentially tens to hundreds of times higher than those of the less accurate method [3].

In this study, two distinct approaches were employed for generating datasets for the Saab 340B passenger aircraft: the semi-empirical DATCOM method and the linear flow solver AVL. The AVL is a vortex lattice method is originally developed in 1988 by MIT's Mark Drela and Harold Youngren. A detailed explanation of the solvers' summaries, simplifications, and restrictions can be found in [4] [5]. Moreover, a comparative analysis is conducted between the outcomes derived from AVL and DATCOM simulations focusing on the clean configuration, and those obtained through Computational Fluid Dynamics (CFD) investigations from [6] . In this paper, Similar investigation and comparison approaches are employed as references. In this academic paper, similar methods of investigation and comparison are used as referenced in [7, 8].

Data fusion is one of the functional approaches to obtain aerodynamic dataset. Since using only high-fidelity wind tunnel test or high-fidelity computational analysis for the aerodynamic dataset generation is expensive to perform in terms of cost, time, or resources. The main motivation of data fusion is to achieve high-fidelity data in a cheaper fashion where low-fidelity aerodynamic data provides the trend information.

This paper presents a follow-up study from a prior works [9] [10]. Reference [9] showed the comparison of two different data fusion techniques being "Variable-Complexity Modelling" (VCM) [11] and co-Kriging method [12] [13]. These methods are widely used due to its simplicity and efficiency, in which the modeling efficiency is higher and the modeling time is shorter [12] [14]. However, these methods have limitations in dealing with high-dimensional problems or large-scale data [15], meaning the time-consumption will increase significantly with the increase of training samples. Reference [10] introduced a new technique which is hybridization of feedforward deep neural network method and genetic algorithm. In this study, this technique is selected and called a deep neural-genetic network (DNGN).

The rest of the paper is organized as follows: Section II presents the DNGN approach. Section III discusses the DOE methods. The results and discussion are presented in Section V. And finally, conclusions are drawn, and future works are given in Section VI . The definition of various aircraft's geometric and other dimensional parameters has been given in the appendix.

II. The Aircraft and Data Preparation

The Saab 340B aircraft, see Figure 1.a, within the National Flying Laboratory Center (NFLC) at Cranfield University is a national resource for the United Kingdom. It is used by several universities across the country to carry out flight tests and provide an experience-based learning opportunity to students. It is also used to carry out experimental work for research undertaken by various institutions. A flight dynamics simulation model of the aircraft

high-fidelity simulation model of this aircraft will further benefit the research work being carried out on Saab 340B aircraft which can be used in the flight simulators such as Cranfield's Future Systems Simulator, see Figure 1.b.

(a) NFLC's Saab 340B aircraft (b) Cranfield University's Future Systems Simulator

Figure 1 NFLC Saab aircraft and FSS Simulator

The main geometry of Saab 340B is shown in Figure 1 . The geometry was taken from grabCAD and some modifications were made for wings, elevators and rudder.

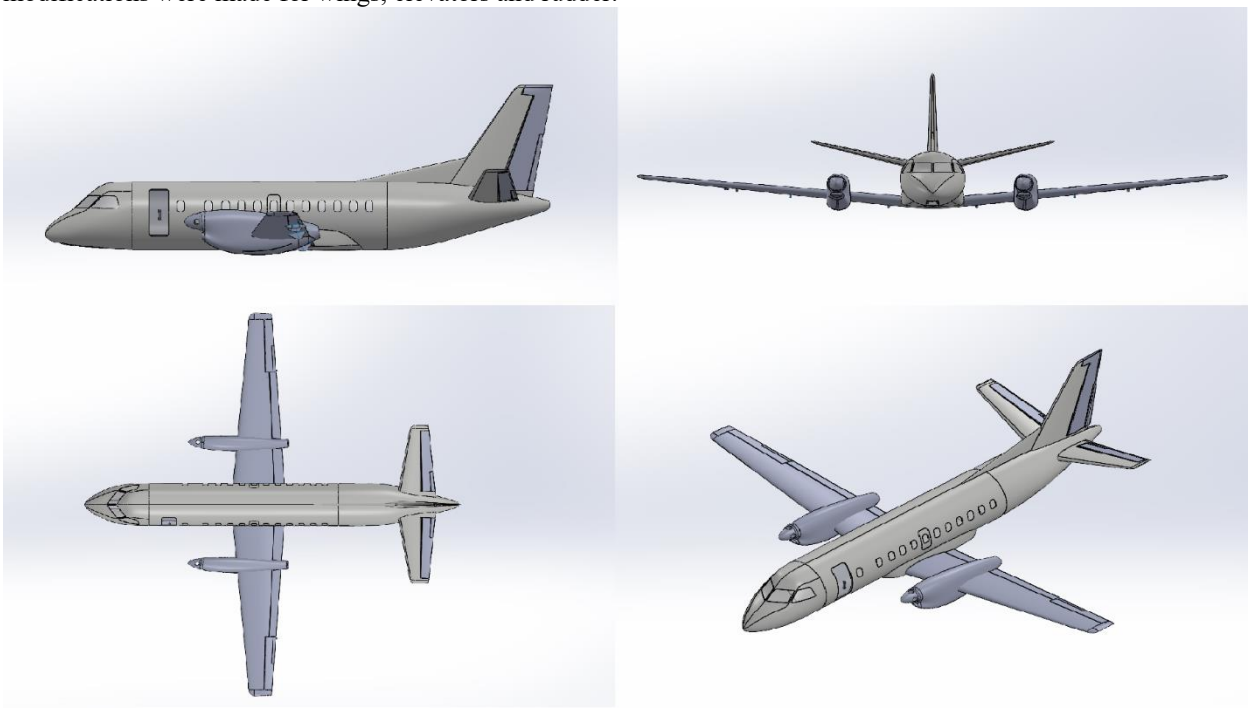

Figure 2 Top, isometric, bottom, and left-side view of SAAB 340B geometry.

The aerodynamic database is created as a function of angle of attack for different horizontal tail deflections in clean configuration. The angle of attack ranges between -9° and 17° while the Mach number is set to 0.2 at sea level flight condition. For the non-dimensional coefficients, the mean aerodynamic chord is selected as 2.45 m while the span is set to 21.44 m. Additionally, the wing area is set to 41.8 m^2. For additional geometric properties, the reader can check Appendix A.

In this paper, datasets are obtained from three-dimensional linear flow solver AVL and semi empirical method DATCOM by using the geometry parameters are obtained from the CAD shown above.

The data encompassed α, δ_e, and δ_{lef}, values in the ranges:

$$\begin{aligned} \alpha &= \{-9°, -7°, -5°, \cdots, 17°\} \\ \delta_e &= \{-22°, -10°, -5°, 0°, 5°, 10°, 18°\} \\ \delta_F &= \{0°, 7°, 15°, 20°\} \end{aligned} \tag{1}$$

A. Athena Vortex Lattice (AVL)

Athena Vortex Lattice is a well-known aerodynamics analysis tool developed by Mark Drela at the Massachusetts Institute of Technology (MIT) based on the code developed by Lamar in NASA [16]. AVL is widely used in the aerospace industry and academia for analyzing the aerodynamic performance of aircraft during the preliminary design phase. AVL relies on the vortex lattice method [5], designed for low Reynolds number flows [17]. Notably, AVL goes beyond the basics by accommodating three-dimensional effects like wing sweep and dihedral angles, providing a more accurate representation of real-world aircraft configurations. AVL also has the capability to model slender bodies like fuselages and nacelles however, there is limited experience with it, so caution is advised when modeling bodies through doublet flow filaments where the flows are circular pattern formed with sources of equal strength, but opposite direction interact, aligning with slender-body theory. If a fuselage has minimal impact on aerodynamic loads, it is simpler to exclude it from the AVL model [18] [4]. AVL offers support for control surfaces and their deflections, allowing for the implementation of multiple control surfaces at specific wing sections, such as a combination of a flap and an aileron. The AVL software is widely used in aerospace research, its strength lies in calculating stability derivatives, making it a common choice for studying flight dynamics. Research articles often focus on smaller airborne platforms, including scale models, drones (UAVs), and micro air vehicles (MAVs)

The process of using AVL begins with users inputting details about the aircraft's geometry, encompassing wing dimensions and tail parameters. Users define the outlining specifics about control surfaces, ailerons, flaps, elevators and rudders and their desired deflections. AVL provides a detailed glimpse into how the aircraft responds to different conditions. The graphical outputs, featuring lift curves, drag polars, and other performance parameters, enhance the visual understanding of the aircraft's aerodynamic characteristics. The tool also generates data files, rich repositories of information that encapsulate the aerodynamic forces and moments at each analyzed condition.

1. Limitations of the AVL

While AVL is a widely used tool for studying aircraft aerodynamics, it comes with certain limitations. It simplifies the air behavior and may be less accurate in certain situations.

a) AVL assumes inviscid flow, neglecting viscous effects. it limits the accuracy of predicting boundary layer behaviors, vorticity shedding, and flow separation. Therefore, AVL is most effective with thin lifting surfaces.
b) AVL method assumes quasi-steady flow conditions, disregarding unsteady effects such as vortex shedding and rapid changes in aerodynamic forces This cause the inaccuracy with high angle of attack or highly dynamic maneuvers [17].
c) AVL has limitations when it comes to capturing the effects of propellers.
d) AVL has limitations concerning compressibility effects as it employs the classical Prandtl-Glauert transformation, assuming incompressible flow. This simplification may result in less accurate predictions, particularly for high-speed flows where compressibility effects become notable. Prandtl-Glauert correction is expressed as:

$$\sqrt{1 - M_\infty^2} \tag{4}$$

where M_∞ is freestream Mach number. PG correction equations are valid up to Mach number 0.6.

2. AVL Setup for Saab340B

The geometry input in the AVL tool involves defining crucial parameters that describe the physical characteristics of the aircraft. This includes specifying details such as the wingspan, mean aerodynamic chord, taper ratio, sweep angle, and dihedral angle for the wings, horizontal and vertical tails, and other components. Additionally, geometric aspects of the fuselage, and control surface deflections are key inputs. These parameters collectively shape the aircraft's configuration, influencing its aerodynamic behavior. Ensuring accurate and comprehensive geometric input is essential for AVL to construct a vortex lattice model, enabling a thorough analysis of the aircraft's aerodynamic

performance during the design and simulation process. Users typically interact with AVL through a graphical user interface or input files, detailing these geometric parameters to derive meaningful insights into the aircraft's behavior.

Within the scope of this paper, the distinctive geometric characteristics of the Saab 340B aircraft, encompassing the wings, horizontal tail, and vertical tail and deflection surfaces such as the rudder, aileron, flap, and elevator, have been integrated into the AVL tool providing representation of the Saab 340B's aerodynamic configuration. These files are available for reference in Appendix B.

a) Geometry Input file

The AVL (Athena Vortex Lattice) geometry input file is a text file that contains essential information about the geometric configuration of an aircraft. This file serves as input to the AVL tool, allowing users to define the key parameters that influence aerodynamic analysis.

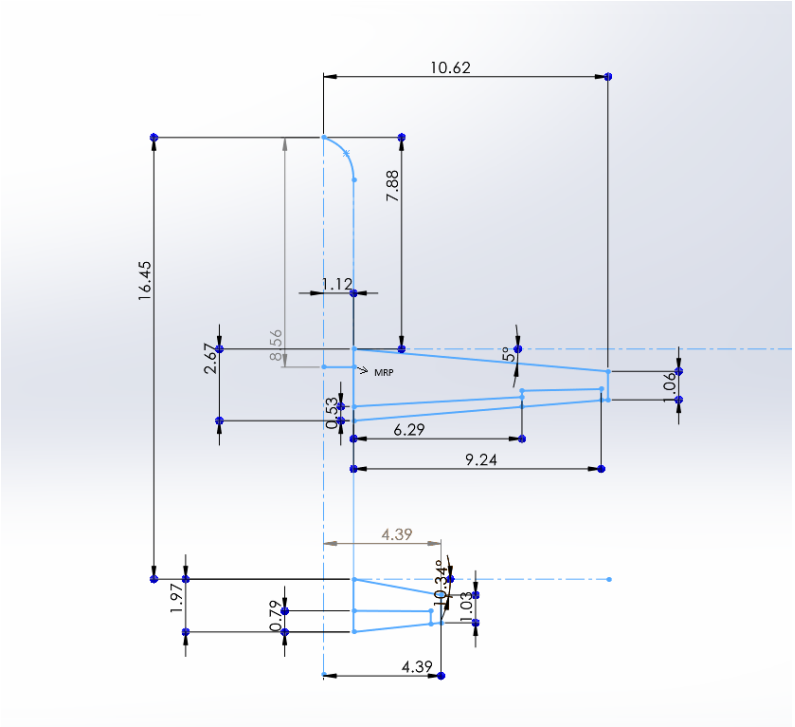

Figure 3 Geometry parameters of the Saab 340B used in AVL input.

Figure 3 illustrates the geometric parameters of the Saab 340B, as referenced in the AVL geometry input file. This visual representation provides a clear overview of the essential characteristics defining the aircraft's configuration within the computational framework of AVL. The depicted geometric parameters, including wingspan, flap, aileron, and rudder details, mean aerodynamic chord, taper ratio, sweep angle, offer valuable insights into the aerodynamic representation utilized for analyses and simulations in AVL. The parameters Nchord, Cspace, and NSpan are used to control the discretization and paneling of the lifting surfaces, allowing users to define the level of detail and accuracy in the aerodynamic analysis. Nchord dictates the number of chordwise panels, determining the resolution along the chord of each surface. Simultaneously, Cspace, a non-dimensional parameter, influences the distribution of chordwise panel spacing, allowing users to adjust the concentration of panels near the wing root. NSpan, on the other hand, specifies the number of spanwise panels, influencing the resolution along the span of each surface. These parameters collectively provide a means for users to decide the level of detail in their aerodynamic simulations. All these inputs can be seen in Appendix B.

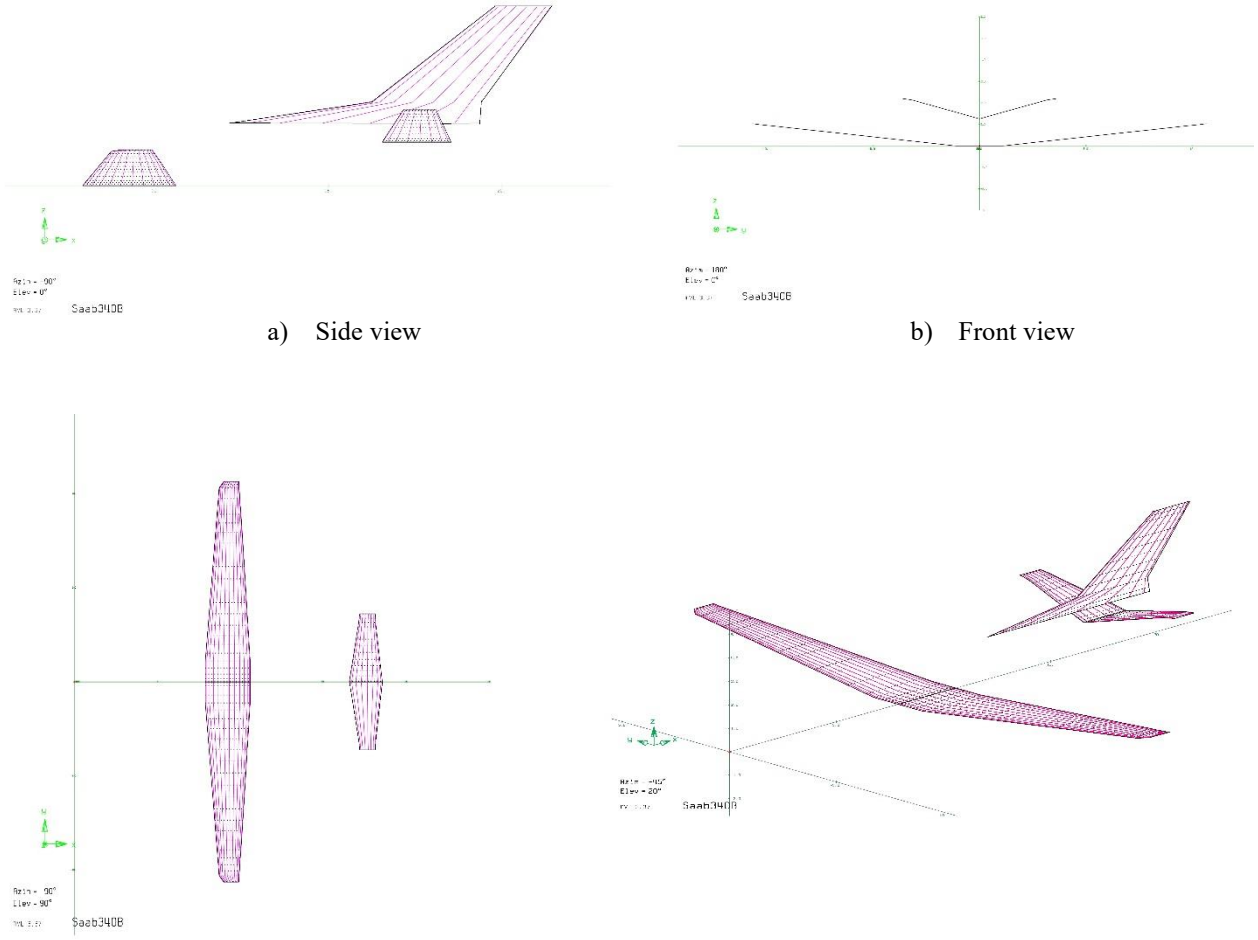

a) Side view

b) Front view

c) Top view

d) İsometric view

Figure 4 Top, isometric, bottom, and left plane view of SAAB 340B in AVL

Figure 4 provides a visual depiction of the Saab 340B's geometric representation within the AVL tool featuring perspectives from the front, left, top, and isometric planes. This illustration serves as a comprehensive visualization, capturing the details of the aircraft's configuration as integrated into the AVL tool.

B. DATCOM

DATCOM, short for "Digital DATa COMpendium," is a widely used tool in aerospace engineering for estimating the aerodynamic characteristics of aircraft. It provides a comprehensive set of aerodynamic data that can be used for preliminary design analysis, performance evaluation, and stability and control assessments. DATCOM was originally developed by the United States Air Force in the 1970s and has since been updated and expanded to accommodate different aircraft configurations. The DATCOM methodology is based on empirical and semi-empirical formulas derived from wind tunnel testing and flight data. It encompasses a range of aerodynamic coefficients such as lift, drag, pitching moment, and control surface effectiveness. These coefficients are determined for various flight conditions, including different angles of attack, sideslip, Mach numbers, and control deflections.

To use DATCOM, like AVL, user input the geometric and physical characteristics of the aircraft, such as wing area, wingspan, fuselage length. The software then computes the corresponding aerodynamic coefficients based on

the provided information and the selected flight conditions. In the application of DATCOM for a passenger aircraft, the input process involves defining key geometric features and flow conditions to assess the aerodynamic behaviour. To initiate this, one must specify essential geometric parameters, encompassing dimensions of the wings, tail, and other pertinent components. Consideration should be given to factors like wing sweep, aspect ratio, and control surfaces such as ailerons and elevators. Furthermore, it is imperative to input relevant flow variables that characterize the operational conditions. These include airspeed, altitude, and Mach number, providing a comprehensive representation of the aircraft's performance envelope. For more information user manual for DATCOM can be useful source. [19]

III.Multi-Fidelity Deep Neural-Genetic Network Algorithm

In this section, the structure of deep neural network and how the genetic algorithm is applied to deep neural network structure are covered.

C. Deep Neural Network Structure

The simplest type of feedforward neural network is the perceptron (artificial neuron), which has only an input layer and an output layer. A perceptron simply has three set of rules; multiplication, summation and activation. In general, mathematical formula of artificial neuron is given in Eq. (2).

$$a = \sigma\left(\left(\sum_i w^i u^i\right) + b\right) \tag{2}$$

where

u^i - the inputs to the artificial neuron
w^i - the weight value corresponding to each input.
b - the bias
σ - the activation function of artificial neuron.
a - the activation (output value) of artificial neuron.

In entrance of perceptron, input vector is multiplied with weight vector, this means that each input has own weight and multiplied with them. This calculation can be called multiplication. In middle section of artificial neuron is sum function that sums all weighted inputs with bias variable. In exit of artificial neuron some specific activation function is applied to previously sum weighted inputs and bias [20]. Figure 5 shows working principle of a single artificial neuron (perceptron).

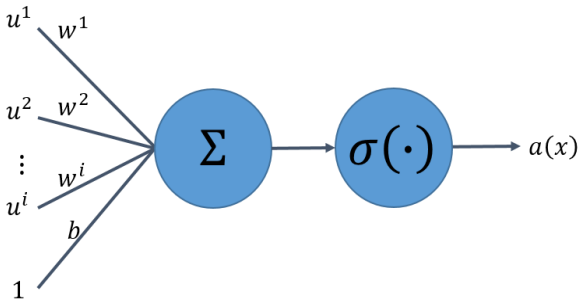

Figure 5 Working principle of a perceptron.

The multi-layer perceptron (MLP) is a feedforward neural network consisting of many perceptron [60]. MLP has three kind of layers; input layer, hidden layer and output layer. Each neural network must has one input and output layer, but they can have many hidden layers. MLP with two or more hidden layers between the input and output nodes

are often classified as feedforward deep neural network or deep neural network [21]. The power of feedforward neural networks to approximate complex nonlinear functions lies in the universal approximation theorem [22]. Simple MLP structure is given Figure 6.

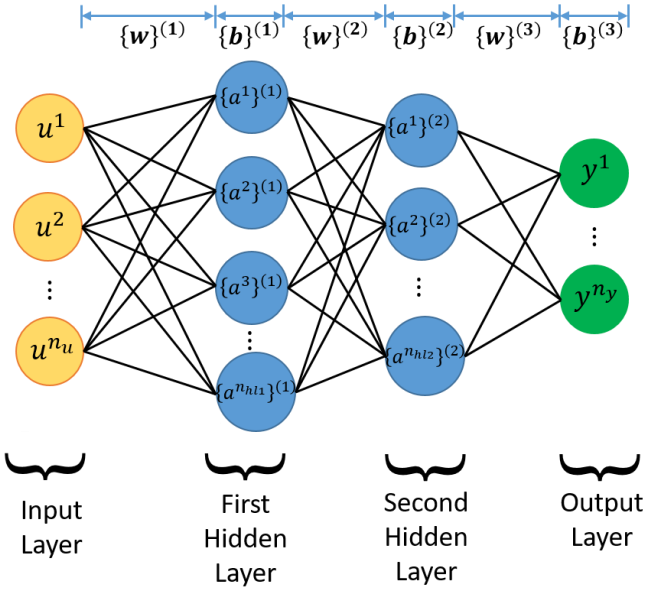

Figure 6 Simple neural network structure.

In Figure 6, there is a typical MLP neural network, which consists of four layers, and these are called the input layer, the first hidden layer, the second hidden layer, and output layer respectively. The output of each layer is obtained as follows:

$$\{a^i\}^{(k)} = \{\sigma\}^{(k)}\left(\left(\sum_j \{w^{ij}\}^{(k)}\{a^i\}^{(k)}\right) + \{b^i\}^{(k)}\right) \tag{3}$$

where

$\{a^i\}^{(k)}$ - the output of i^{th} neuron in the k^{th} layer

$\{w^{ij}\}^{(k)}$ - the weight of the connection from the j^{th} neuron in the $(k-1)^{\text{th}}$ layer to the i^{th} neuron in the k^{th} layer

$\left\{b^i\right\}^{(k)}$ - the bias term of the i^{th} neuron in the k^{th} layer.

$\{\sigma\}^{(k)}$ - the activation function in the k^{th} layer.

We will refer to the activations of the input units as u_j and the activation of the the output units as y_j

$$\{a^i\}^{(0)} = u^i \tag{4}$$

The outputs of the neurons in the last layer can be seen as the overall networks' outputs:

$$y^i = \{a^i\}^{(3)} \tag{5}$$

Activation function used in artificial neuron is key element of neural network. Without activation function neural network cannot learn nonlinear function. Activation function provide neural network some nonlinearities. There are many activation functions used in literature, but most commonly used activation functions are given in Table 1.

Table 1 Most Commonly Used Activation Functions

#	Name	Function
1	Logsig	$\sigma(x) = \frac{1}{1+e^{-x}}$
2	Tansig	$\sigma(x) = \frac{2}{1+e^{-2x}} - 1$
3	Linear	$\sigma(x) = x$
4	ReLU	$\sigma(x) = \max(x, 0)$

A two hidden layer deep neural network with linear transfer function at output layer is selected for this study. And, instead of matching the multiple outputs through a single network, multiple modules are used, each consisting of a suitable neural network characterizing just one aerodynamic coefficient. For regression, we use sum-of-squared errors as our measure of fit (objective function). Mean square error (MSE) method is used for loss calculation of neural network and MSE is given in equation (8)

$$\text{MSE}_{Train} = \frac{1}{n_{data}} \sum_{j=1}^{n_{data}} \left(z_j - y_j \right)^2 \tag{6}$$

i - the neuron index
j - the discrete data index
n_{data} - Number of data
z_j^i - Measured (actual) data of i^{th} neuron in j^{th} discrete data index
y_j^i - Estimated Data of i^{th} neuron in j^{th} discrete data index

Another important concept of neural network is used backpropagation algorithm. Among many backpropagation algorithms, the Levenberg-Marquardt backpropagation algorithm is chosen for this study since it is fast and gives better results [23]. It is combination of Gradient Descent and Gauss-Newton optimization .
Table 2 presents the hyperparameters of the Levenberg-Marquardt Algorithm

Table 2 The Hyperparameters of Levenberg-Marquardt Algorithm

#	Name	Symbol
1	Initial Dampening Factor	μ_0
2	Increase Dampening Factor	μ_{dec}
3	Decrease Dampening Factor	μ_{inc}
4	Maximum Dampening Factor	$\bar{\mu}$

1. Some Issues in Deep Neural Network Training

There are several important issues associated with the setup of the neural network, preprocessing, and initialization. Neural network training can be made more efficient if certain steps are performed for these issues. In this sub-section, several important issues will be described [23] [24].

Scaling of the Inputs and Outputs (Feature Preprocessing)

Data scaling is recommended before applying the optimization methods [25]. This is found to be particularly the case while training feedforward neural networks. Here, scaling refers to arranging the values between the chosen lower and upper limits such that all of the variables have similar order of magnitudes. All data is scaled to the range [0,1] or [-1,1] generally [23] [25] [26] [27]. For this study, all data is scaled to the range [-1,1] to reduce numerical error during neural network training as recommended by [23].

$$\boldsymbol{u}_n^i = -1 + \frac{2\left(\boldsymbol{u}^i - \boldsymbol{u}_{min}^i\right)}{\boldsymbol{u}_{max}^i - \boldsymbol{u}_{min}^i}$$
$$\boldsymbol{y}_n = -1 + \frac{2(\boldsymbol{y} - \boldsymbol{y}_{min})}{\boldsymbol{y}_{max} - \boldsymbol{y}_{min}} \tag{7}$$

where $(\quad)_{min}$, $(\quad)_{max}$, and $(\quad)_n$ are the minimum, maximum, and normalized value of the considered variable respectively.

The initial weights

Initial weight assignment is one of the most important steps in neural network setup. The initial weights are normally set to small random numbers to avoid saturation in the neurons. It was observed that the algorithm does not work properly if the initial weights are either zero or poorly chosen nonzero values [25]. Use of exact zero weights leads to zero derivatives and perfect symmetry, and the algorithm never moves. Starting instead with large weights often leads to poor solutions [28]. To avoid the saturation region of the activation function, the weighted sum output value will be near to 0 as much as possible, which can increase the weight adjustment range. Therefore, the initial connection weights are usually random numbers between [-1,1] so that the network will not be greatly affected [29].

In this study, initial weights and bias are set between random numbers between [-1,1] and scaled by scale factors between [0,1].

2. Feedforward deep neural network model validation

The performance of the neural network is an important criterion to assess the optimized hyperparameters. The available dataset is divided into training and testing dataset, firstly. The testing dataset, which is not seen in the identification phase, is used to assess the final performance at the end of the model identification. However, we should remark that in the identification phase, the training dataset can be used in different ways in order to assess the fitted model using various resampling methods. e.g., train-validation split (hold-out cross-validation), k-fold cross-validation, or bootstrap approaches. The simplest one is the hold-out cross-validation approach. This approach randomly divides the training dataset into two groups: training and validation datasets. This approach has a potential drawback; the estimated test error rate can be highly variable depending on which observation dataset falls into the training dataset and which observation falls into the validation dataset. Thus, it is a good practice to apply other resampling methods as a refinement to overcome this drawback; some of them are K-fold cross-validation and bootstrap approaches. It was shown that the k-fold cross-validation approach is superior to hold-out cross validation and bootstrap approaches [30].

The test set error is not used during the training, but it is used to compare different models. It is also useful to plot the test set error during the training process. If the error in the test set reaches a minimum at a significantly different iteration number than the validation set error, this may indicate a poor division of the data set [23].

For this study, dataset is divided two part; training (80%), testing (20%) and k-fold cross-validation approach is used to validate the neural network.

D. Hyperparameter Optimization Methods

The hyperparameters that define a deep neural network can be separated into two categories: the ones that define the architecture of the network and the ones that affect the optimization process of training phase. The proposed method considers both categories at once.

Tuning the hyperparameters of a deep neural network is a critical process that was mainly done manually relying on the previous experience of the experts (manual search). This is usually done using a trial-and-error process. However, even with expertise in deep neural network and its hyperparameters, the best settings of these hyperparameters will change with different data and time consuming. To address this problem, the ability to find the optimal hyperparameters in an automated manner is needed. Since genetic algorithm theory is mature and widely used optimization routine, the automated hyperparameter selection in Deep Neural Network is done via genetic algorithm.

1. Genetic Algorithm

Genetic algorithms are optimization methods that are inspired by biological evolution. Genetic algorithms operate on a population of candidate solutions and apply the principle of survival of the fittest to evolve the candidate solutions towards the desired optimal solutions. In genetic algorithm, candidate solutions are referred to as individuals or parameters. A population refers to the group of individuals. The reader is referred to Refs. [31] [32] [33] [34] for detail description of genetic algorithms. Figure 7 illustrates the steps of typical genetic algorithm.

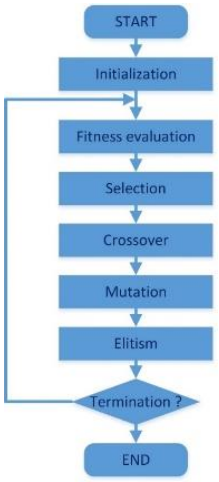

Figure 7 Typical Genetic Algorithm Flowchart

E. Hybridization of Genetic Algorithm with Deep Neural Network

Figure 8 shows a deep neural network flowchart. The measured output and predicted output are compared and an objective function is measured to evaluate the performance of neural network. Weights and biases are updated using solver (optimization) algorithm to minimize the objective function. Neural Network architecture/solver hyperparameters and initial weights/biases must be decided before the optimization routine starts.

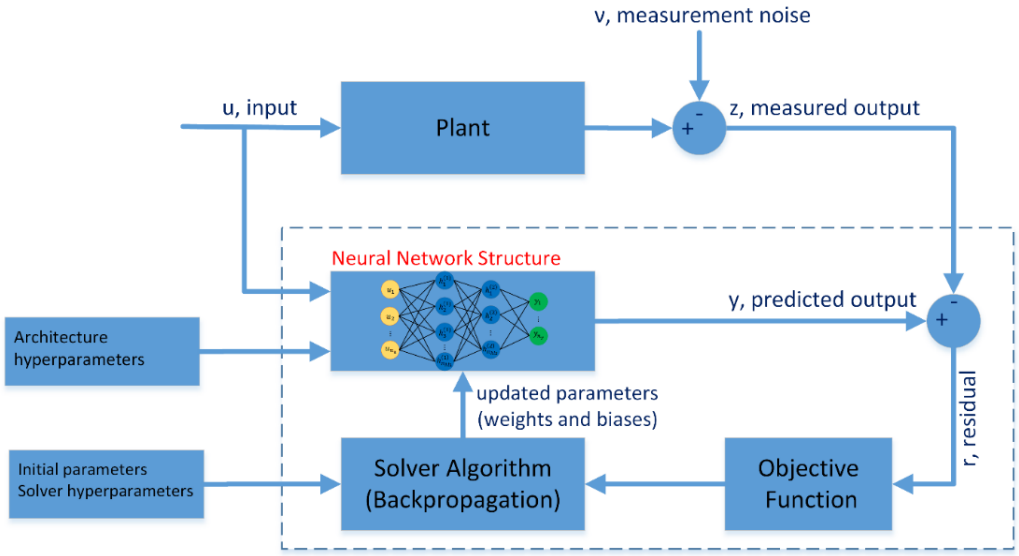

Figure 8 Deep Neural Network Flowchart

Table 3 and Table 4 summarize the hyperparameters responsible for defining the structure of the network.

Table 3 User Defined Neural Network Hyperparameters

#	Hyperparameter	Ranges and Functions
1	Architecture	2 hidden layer feed forward neural network
2	Fitness function	Training dataset MSE
3	Solver	Levenberg-Marquardt Optimization
4	Epoch	300
5	Maximum dampening factor for solver, $\bar{\mu}$	10000

Table 4 Neural Network Hyperparameters Tuned by Genetic Algorithm

#	Hyperparameter	Ranges and Functions
1	Number of neurons in the first hidden layer	{1,2,…,50}
2	Activation function for the first hidden layer	{Logsig, Tansig, ReLU, Linear}
3	Number of neurons in the second hidden layer	{1,2,…,50}
4	Activation function for the second hidden layer	{Logsig, Tansig, ReLU, Linear}
5	Weights and biases initization factor	[0,1]
6	Initial Dampening factor for solver, μ_0	{0.01, 0.02, …, 0.1}
7	Increase factor for solver, μ_{inc}	{2, 3, …, 10}
8	Increase factor for solver, μ_{dec}	$\{1/2, 1/3, \ldots, 1/10\}$

F. Multi-Fidelity Deep Neural-Genetic Network Algorithm Implementation

The implementation of MFDNGN algorithm is as follows:

1. Low-fidelity DNGN model is build using low-fidelity dataset.

$$f(u_{LF}) \approx f_{LF}(u_{LF}) \tag{8}$$

2. Predict low-fidelity values for each data point in high-fidelity dataset. This step is necessary, because given dataset probably is not taken in the same aerodynamic condition.

$$f(u_{HF}) \approx f_{LF}(u_{HF}) \tag{9}$$

3. At each high-fidelity data point, the increments or differences are calculated between low-fidelity data which calculated in step-2 and high-fidelity data.

$$\beta(u_{HF}) = f_{hf}(u_{HF}) - f_{lf}(u_{HF}) \tag{10}$$

4. Increment function in Eq. (7) is calculated by interpolating the set of increments or differences data which are found in step-3 using DNGN approach.

5. Data fusion function in Eq. (6) is simple summation of low-fidelity Kriging and increment Kriging model for desired data point.

$$f(x) \approx f_{lf}(x) + \beta(x) \tag{11}$$

When the broad range of aircraft flight envelope is considered, these aerodynamics coefficients have nonlinear relationships with their dependent variables. The two separate fully-connected neural networks can be employed to approximate the linear and nonlinear part of increment function for the low- and high-fidelity data [35]. But in order to reduce the computational effort, the nonlinearity in the increment function is expressed by using spline functions. Spline functions are defined only on the subintervals, and can approximate nonlinearities quite well. The angle of attack range is divided and added as dependencies to neural network inputs for improving performances. Parameters dependent on the angle of attack in longitudinal coefficients are expressed using spline functions [36] in the form

$$(\alpha - \alpha_i)_+^m = \begin{cases} (\alpha - \alpha_i)^m & \alpha \geq \alpha_i \\ 0 & \alpha < \alpha_i \end{cases} \tag{12}$$

IV.Design of Experiment Methods

Experiment design method is a key to construct a highly reliable models for numerical optimization in large-scale project. Within the method, the experimental design criterion directly affects the accuracy of the model and the optimization efficient. Random sampling, Latin hypercube, Halton and Sobol sequences are the traditional design of experiment methods. These methods can also be called space filling methods. Space filling methods are based on spreading the samples around the design space without following a specific factor levelling schema. The number of selected samples is predefined by the designer and does not depend on the number of the problem factors.

Random sampling is just randomly selection of samples in design space. It is easy to obtain and use randomly sampled design points. Therefore, it is very useful for beginning analysis. When sample points are large enough, random sampling method is useful. However, randomly sampled small number of points in design space don't be distributed reasonably. If there are large design points, random sampling can be used as design of experiment method. It is widely used, because, it is easy to use, fast and quickly obtained. On the other side, if design points are not enough, random sampling is not recommended. In random sampling, new sample points are generated without taking into account the previously generated sample points.

Latin hypercube is statistical method for generating a near-random sample of parameter values. In Latin hypercube sampling technique, samples are selected according to a uniform distribution. Unlike random sampling methods, Latin hypercube sampling, takes out the previous generated point location in order to generated new point location. So it has less point to express design space. Latin hypercube mostly used in Monte Carlo simulation. Because, it reduces the number of runs for successfully achieve reasonable results. Typically, Latin hypercube sampling is used to reduce computational cost of Monte Carlo simulations. In this study, Latin hypercube is used to reduce number of necessary high fidelity points. Therefore, using Latin hypercube sampling, provide us, more coverage of design space with using less number of data points. Latin hypercube ensure that the entire range of each design space is completely covered without regard to which single design variable or combination of design variables dominate the design points.

In statistic, Halton sequences are sequences used to generate points in space for numerical methods such as Monte Carlo simulations. Halton method was introduced in 1960, and are an example of a quasi-random number sequences. Halton and Sobol sequence sampling provide a lower discrepancy (they fill the design space of possibilities more

evenly) resulting in more reasonable design point in the case of expression of all high-fidelity points. Sobol sequence was invented in USSR in 1967 and its computation was massively improved in 1979 by Antonov and Saleev. As a result of these studies, a reasonable effective Sobol sequence sampling method is developed. Sobol sequence sampling is remarkable efficient in the case of low dimension design space, on the other hand, in the case of high dimension, Sobol sequence is unsuitable.

V.Results and Discussions

A. Comparison of the AVL, DATCOM and CFD Results for clean configuration.

The graphs presented appear to be a comparison of aerodynamic coefficients obtained from different analysis methods: Computational Fluid Dynamics (CFD), Athena Vortex Lattice (AVL), and DATCOM for a certain clean configuration of an aircraft. Each graph shows a different relationship between aerodynamic coefficients and angle of attack (α).

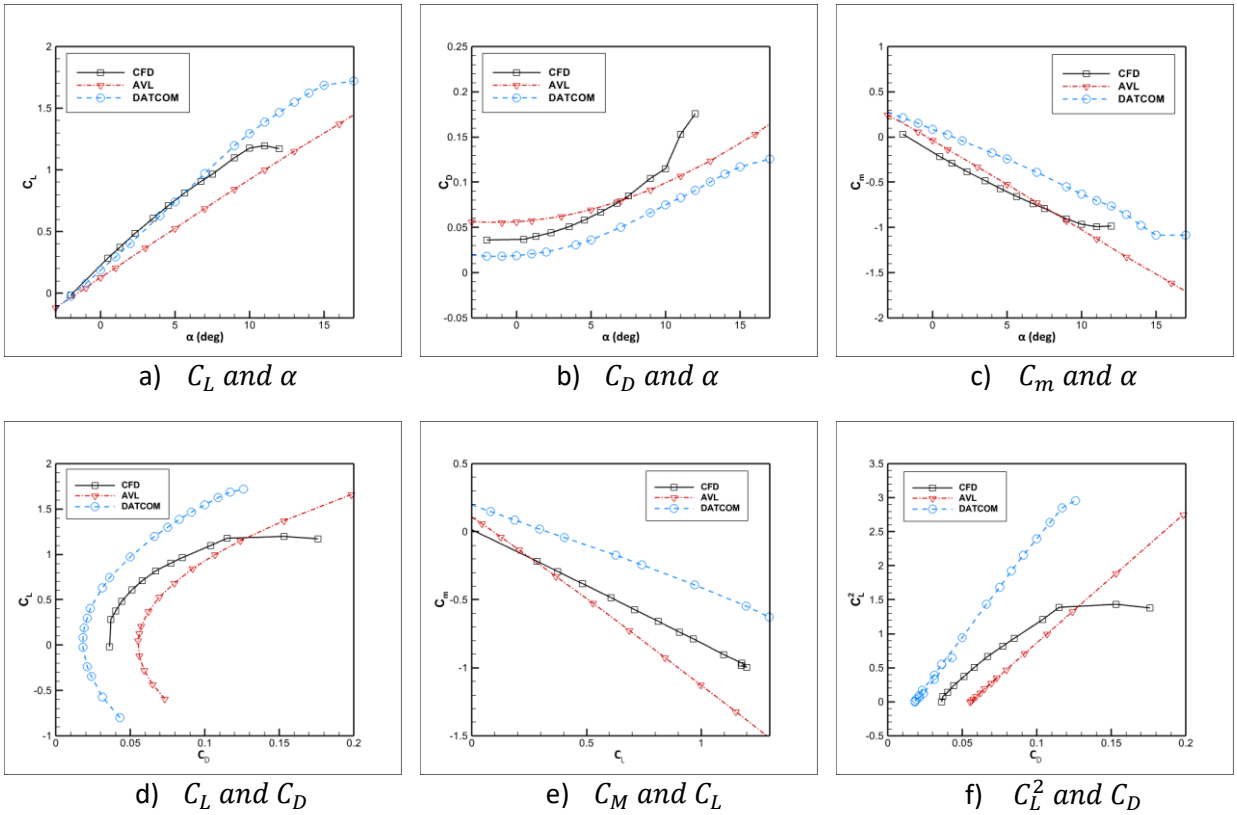

Figure 9 Comparative analysis of lift C_L, drag C_D, and moment C_m coefficients as functions of angle of attack (α), and the inter-relationships between these coefficients for an aircraft in a clean configuration, using AVL, DATCOM, and CFD simulations. [6].

Figure 1a illustrates the variation of the lift coefficient as the angle of attack increases. The lift coefficient increases with the angle of attack for all three methods, indicating a typical aerodynamic behavior where lift increases with an increase in α until it reaches a critical point leading to stall. The CFD data shows a slightly higher lift generation capability, which may suggest a more optimistic prediction of the stall angle, or a different treatment of the boundary layer effects compared to AVL and DATCOM. Moreover, as it is seen from the Figure 9b the drag coefficient also rises with increasing angle of attack, reflective of the growing air resistance as the aircraft presents a larger profile to the oncoming air. The close agreement between AVL and DATCOM may indicate a similar approach in estimating parasitic and induced drag components at lower angles. The divergence of CFD data at higher angles could be attributed to the method's ability to capture complex flow phenomena like separation and vortex shedding, which typically increase drag. Figure 9c indicates that the moment coefficient's negative slope with respect to α across all methods suggests a nose-down pitching moment that increases as the aircraft's angle of attack rises. This is typical of

aerodynamically stable aircraft configurations. In Figure 9a, b, The linear trend in the C_m and C_L versus angle of attack (α) depicted by AVL suggests its simplified flow assumptions, likely not accounting for non-linear aerodynamic phenomena such as flow separation, which are captured in the non-linear trends shown by DATCOM and CFD. This difference highlights AVL's limitations in predicting complex aerodynamic behaviors at higher angles of attack, where empirical and computational methods like DATCOM and CFD offer more accurate representations due to their inclusion of real-world aerodynamic effects [1]. Figure 9Figure **9** shows that the lift coefficient C_L against drag coefficient C_D graph reveals the aerodynamic efficiency of the aircraft. All methods suggest a similar trend where efficiency increases up to a certain point before decreasing, with DATCOM predicting a higher peak efficiency. The graph plotting C_m against C_L Figure 9e illustrates the stability characteristics of the aircraft. The CFD data suggests less stability at higher lift coefficients compared to AVL and DATCOM. Finally, the squared lift coefficient C_L^2 plotted against C_D represents the aerodynamic performance in terms of glide ratio. The CFD results indicate a superior glide performance, with a higher C_L^2 for a given C_D.

B. Longitudinal AVL and DATCOM simulations

1. *Flap Deflections*

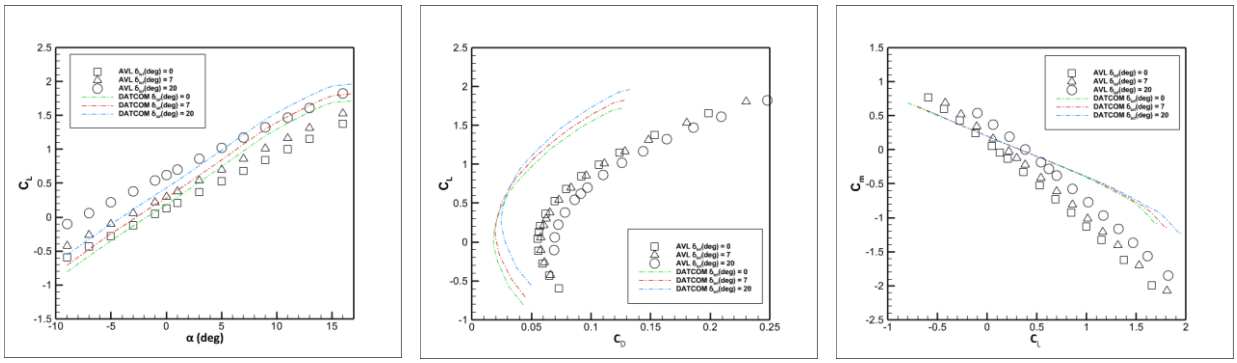

a) C_L *and* α *with* δ_{lef} *for AVL and DATCOM*

b) C_L *and* C_D with δ_{lef} for AVL and DATCOM

c) C_M *and* C_L *with* δ_{lef} *for AVL and DATCOM*

Figure 10 Aerodynamic coefficient analysis comparing the effects of flap deflection on lift C_L, drag C_D and pitching moment $C_m$coefficients, using AVL and DATCOM simulations. The graphs show the influence of various flap deflections on these coefficients.

Figure 10a illustrates the effect of flap deflections on the lift coefficient across a range of angles of attack. Both AVL and DATCOM show that as the flap deflection increases, the lift coefficient also increases, which is consistent with expected aerodynamic behavior. For each flap deflection angle, there is a corresponding increase in lift, with AVL and DATCOM results closely aligned at lower deflections and showing slight divergence at higher deflections. This graph represents the aerodynamic trade-off between lift and drag as the flaps are deflected. In Figure 10b for both AVL and DATCOM, the data indicates that with increased flap deflection, the drag coefficient increases along with the lift coefficient. This is a typical outcome as flaps increase the camber of the wing, enhancing lift at the cost of increased drag. Figure 10c shows the AVL and DATCOM simulations exhibit the expected increase in negative pitching moment coefficient with higher lift coefficients as flap deflection increases, indicative of a nose-down moment.

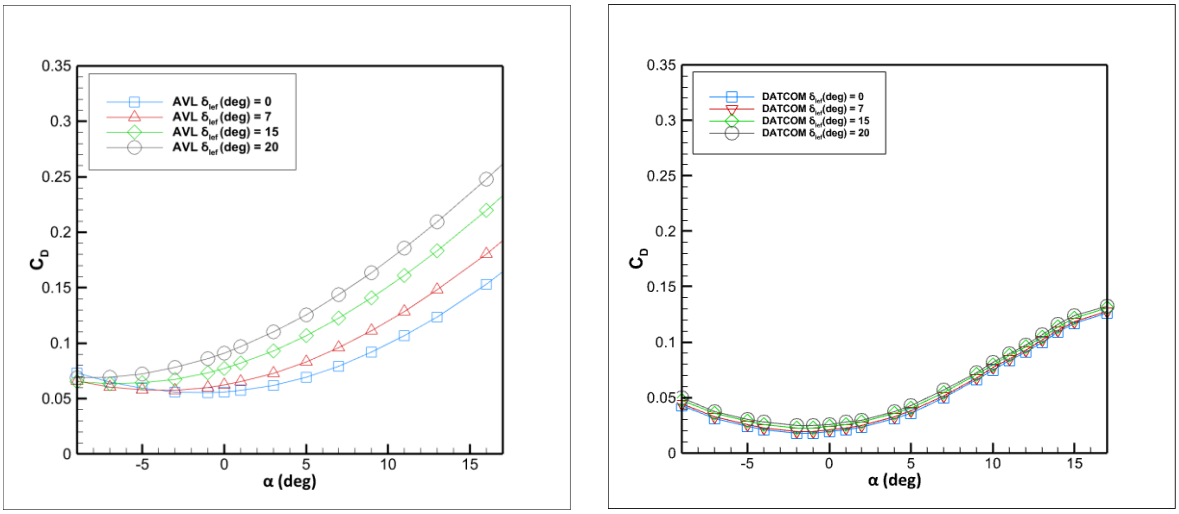

a) C_D *and* α *for AVL with* δ_{lef}

b) C_D *and* α *for DATCOM with* δ_{lef}

Figure 11 Comparative assessment of drag coefficient C_D responses to angle of attack (α) and flap deflection (δ_{lef}) using AVL and DATCOM simulations, highlighting the differential predictive behaviors of these two aerodynamic analysis tools.

From the Figure 11a the AVL simulation demonstrates that the drag coefficient increases with the angle of attack, with increasing flap deflection, the drag coefficient rises, particularly at higher angles of attack. The curves also show a non-linear growth in drag, more pronounced with greater flap deflections, indicating a non-linear relationship between drag and flap deflection as well as the angle of attack. The DATCOM simulation presents a similar trend where the drag coefficient rises with an increase in angle of attack and flap deflection. However, the curves appear to be closer together compared to the AVL results, suggesting that the increase in drag due to flap deflection is less pronounced in the DATCOM simulation.

2. Elevator Deflections

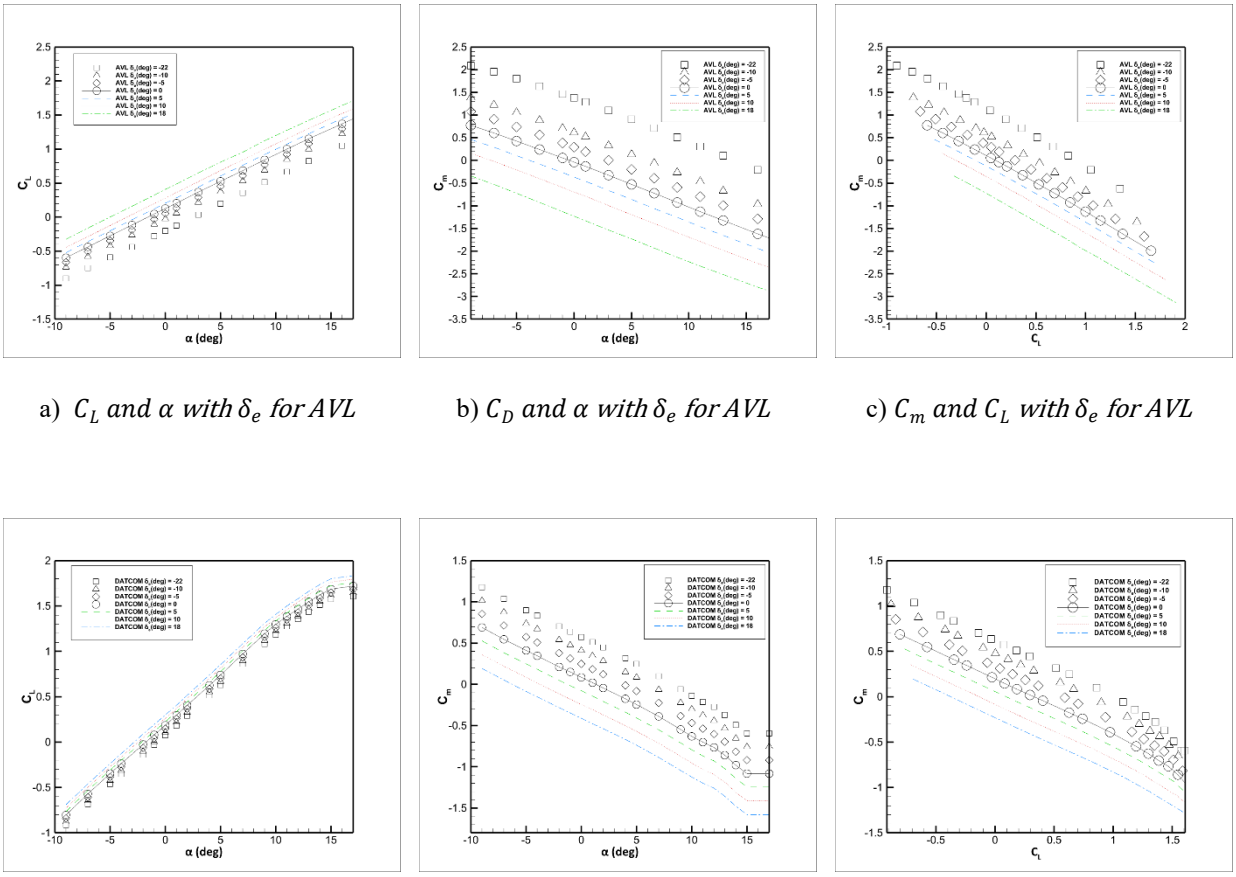

a) C_L *and* α *with* δ_e *for AVL*

b) C_D *and* α *with* δ_e *for AVL*

c) C_m *and* C_L *with* δ_e *for AVL*

d) C_L *and* α *with* δ_e *for AVL*

e) C_D *and* α *with* δ_e *for AVL*

f) C_D *and* α *with* δ_e *for AVL*

Figure 12 Comparative analysis of the effects of elevator deflections on aerodynamic coefficients using AVL and DATCOM simulations. The graphs demonstrate the relationship between lift (C_L), drag (C_D), and pitching moment (C_m) coefficients with varying angles of attack (α) and elevator deflections (δ_e), reflecting the critical role of elevator position in controlling aircraft pitch and lift, with minimal influence on drag.

Figure 12 shows that both AVL and DATCOM C_L increases linearly with angle of attack (α) for various elevator deflections (δ_e), suggesting a consistent response to angle changes regardless of the control surface position. However, AVL simulations exhibit a slightly more pronounced deviation between the lines representing different (δ_e) values. This could indicate a greater sensitivity of the AVL model to the effects of elevator deflection on the lift generated by the aircraft. In terms of drag, both models demonstrate that the primary driver of C_D is the angle of attack rather than elevator deflection. The minimal influence of δ_e on drag is consistent across both AVL and DATCOM However, small differences can be observed in how each model predicts the changes in C_D with δ_e, with AVL showing a steeper gradient. For the pitching moment, both simulations confirm the expected trend: as the lift coefficient increases, a downward deflection of the elevator increases the nose-down pitching moment.

C. Comparison of Design of Experiment Approaches

The MSE and R2 of the testing high fidelity data with different DOE approaches are listed in Table 5.

Table 5 MSE and R^2 of the testing high fidelity dataset with different methods for 60% percentage of high-fidelity dataset

Set	Approach	Mean Square Error (MSE)			Coefficient of Determination (R^2)		
		C_D	C_L	C_m	C_D	C_L	C_m
High-Fidelity Test Dataset	Latin Hypercube	0.00002	0.00056	0.00008	0.99976	0.99743	0.99609
	Halton Sequences	0.00002	0.00005	0.00010	0.99978	0.99979	0.99545
	Sobol Sequences	0.00009	0.00012	0.00002	0.99887	0.99944	0.99894

For the rest of the study, Halton Sequences is selected as DOE in lift and drag coefficients, whereas, Sobol is selected as DOE in pitch moment coefficient. Since the MSE is the lowest for those DOE techniques.

Figure 13 shows the linear regressions of true and predicted aerodynamic coefficients for different DOE techniques for 60% percentage of high-fidelity datasets.

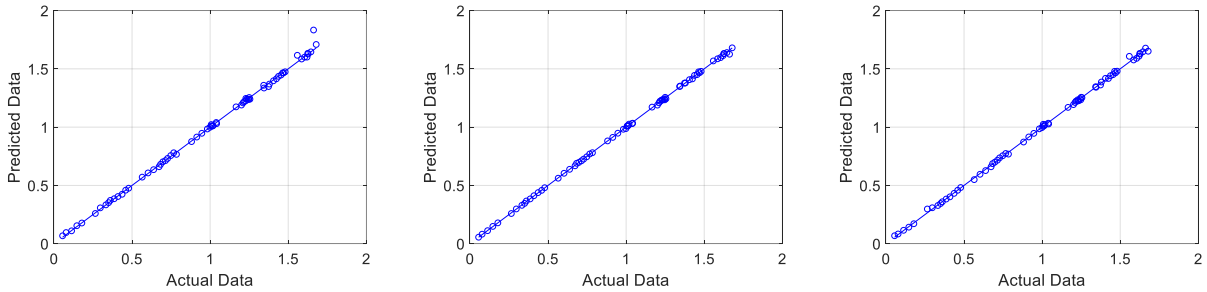

a) Latin Hypercube Sampling b) Halton Sequences c) Sobol Sequences

Figure 13 Accuracy spread of the high-fidelity testing points of C_L with different DOE techniques

VI. Conclusion

A Saab 340B aircraft geometry is obtained from publicly open resources and its geometric details are corrected. Datcom input file is created and subsonic aerodynamic database of Saab 340B is generated for the baseline and deflected elevator configurations. Across the various analyses using AVL, DATCOM and CFD, a consistent trend emerges showing the impact of control surface deflections on aerodynamic coefficients. While all methods agree on the general effects of flap and elevator deflections on lift (C_L), drag (C_D), and pitching moment (C_m), the degree of sensitivity varies. AVL appears to be more responsive to changes in control surface deflections, suggesting a higher resolution in capturing aerodynamic nuances, particularly in lift and pitching moment predictions. DATCOM tends to present a more conservative approach, with closer grouping in drag predictions across different flap deflections. CFD simulations provide a more detailed picture, capturing non-linear behaviors and complex flow phenomena, especially at higher angles of attack. These variations highlight the importance of selecting appropriate aerodynamic prediction tools based on the specific design and analysis requirements, and the need for corroborative data from multiple simulation methods to ensure comprehensive aerodynamic performance understanding.

The Deep Neural-Genetic Network approaches are used to derive high-fidelity datasets using more low-fidelity dataset and less high-fidelity dataset to reduce the computational cost of high-fidelity dataset generation. The MSE and R2 results obtained for the lift, drag and pitch moment coefficient are compared for various Design of Experiment techniques. The Halton Sequence is superior to other approaches for lift and drag coefficients in terms of MSE and R2, whereas Sobol Sequence yields the best result for pitch moment coefficient in terms of MSE and R2.

Experiment design is the key factor for the surrogate prediction accuracy. Traditional experimental design suffers blindness to a certain extent and large wasted analysis time for sampling. As a future work, an improved sampling methods (based on Ref. [37]) will be implemented to solve the shortcomings of the traditional experimental designs in this paper. Also, the effect of aileron, rudder and slipstream effects will also be included in the final manuscript. It is also expected to conduct wind tunnel testing and incorporate hierarchical multi multi-fusion approach

VII.References

[1] B. Peerlings, "A review of aerodynamic flow models, solution methods and solvers and their applicability to aircraft conceptual design," Delft University of Technology, Delft, 2018.

[2] M. Tyan, M. Kim, V. Pham, C. Choi, L. Nguyen and J. W. Lee, "Development of Advanced Aerodynamic Data Fusion Techniques for Flight Simulation Database Construction," in *AIAA Aviation Forum*, Atlanta, GA, 2018.

[3] Q. Liu, P. Zhang, W. Xiao and J. D. Diao, "Correction Methods of Aerodynamic Force and Moment Coefficients Based on the Identification Data," in *Chinese Control Conference*, Guangzhou, China, 2019.

[4] Drela M. and Youngren H., "AVL 3.30 User Primer, Technical Report," Massachussets Institute of Technology, Massachussets, United States of America, 2010.

[5] M. Drela, Flight Vehicle Aerodynamics, London: The MIT Press, 2014.

[6] L. Li, "Master Thesis A numerical Study of the Aerodynamics of the Saab 340B," Cranfield Univeristy, 2022-2023.

[7] Fabrizio Nicolosi, Pierluigi Della Vecchia, Salvatore Corcione, "Design and aerodynamic analysis of a twin-engine commuter aircraft," *AerospaceScienceandTechnology,* pp. 1-16, 2015.

[8] Fabrizio Nicolosi, Salvatore Corcione and Pierluigi Della Vecchia, "Commuter aircraft aerodynamic," *Aircraft Engineering and Aerospace Technology: An International Journal,* pp. 523-534, 2016.

[9] H. B. Kurt, M. Millidere, F. S. Gömeç and Ö. Uğur, "Multi-fidelity Aerodynamic Dataset Generation of a Fighter Aircraft," in *AIAA Scitech Forum*, Virtual Event, 2021.

[10] M. Millidere, F. S. Gömeç, H. S. Kurt and F. Akgül, "Multi-Fidelity Deep Neural Network Method of Aerodynamic Database Generation for a Fighter Aircraft," in *AIAA Aviation Forum*, Virtual Event, 2021.

[11] C. Tang, K. Gee and S. Lawrence, "Generation of Aerodynamic Data Using a Design of Experiment and Data Fusion Approach," in *AIAA Aerospace Science Meeting and Exhibit*, Reno, NV, 2005.

[12] A. Forrester, A. Sobester and A. Keane, Engineering Design via Surrogate Modelling: A Practical Guide, A John Wiley and Sons Inc, 2008.

[13] A. Forrester, A. Sobester and A. Keane, "Multi-fidelity optimization via surrogate modelling," *Proceedings of the Royal Society: A Mathematical, Physical and Engineering Sciences,* vol. 463, no. 2088, pp. 3251-3269, 2007.

[14] J. Laurenceau and P. Sagaut, "Building Efficient Response Surfaces of Aerodynamic Functions with Kriging and Cokriging," *AIAA Journal,* 2008.

[15] P. Perdikaris, M. Raissi, A. Damianou and G. E. Karniadakis, "Nonlinear information fusion algorithms for data-efficient multi-fidelity modelling.," *Proc. Math. Phys. Eng. Sci.,* 2017.

[16] L. E. J., "A Vortex-Lattice for of the Mean Method Shapes of Trimmed Noncoplanar Planforms," Technical Report NASA TN D-8090, National Aeronautics and Space, Hampton, Unıted States of America, 1976.

[17] Thomas P. R. Richardson T. S., "Estimation of Stability and Control Derivatives for a Piper," in *In AIAA Modeling and Simulation Technologies Conference*, Minneapolis Minnesota, 2012.

[18] Rose M., Yaralian H., Wagster H., Bhandari S., "Development and Validation of Flight," in *In Infotech@Aerospace 2012*, Gardem Grove, United States of America, 2012.

[19] "THE USAF STABILITY AND CONTROL DATCOM," McDonnell Douglas Astronautics Company, St Louis, Missouri, 1979.

[20] A. Krenker, J. Bester and A. Kos, "Introduction to the Artificial Neural Networks – Methodological Advances and Biomedical Applications," IntechOpen, Kenji, Suzuki, ???.

[21] H. S. Das and P. Roy, in *A Deep Dive Into Deep Learning Techniques for Solving Spoken Language Identification Problems*.

[22] A. S. Tenney, M. N. Glauser and Z. P. Berger, "Application of Artificial Neural Networks to Stochastic Estimation and Jet Noise Modeling," *AIAA Journal,* 2010 ???.

[23] H. Demuth and M. Beale, "Neural Network Toolbox," The MathWorks, Natick,MA, 2004.

[24] C. C. Aggarwal, Neural Networks and Deep Learning, Yorktown Heights, NY: Springer, 2018.

[25] R. V. Jategaonkar, Flight Vehicle System Identificiation: A Time-Domain Methodology, Reston, VA: AIAA Process in Astronautics and Aeronautics, AIAA, 2015.

[26] T.-A. Nguyen, H.-B. Ly and B. T. Pham, "Backpropagation Neural Network-Based Machine Learning Model for Prediction of Soil Friction Angle," *Hindawi Mathematical Problems in Engineering,* 2020.

[27] I. H. Witten, E. Frank and M. A. Hall, "Data Management Systems," in *Chapter 7- data transformations*, Burlington, MA, Morgan Kaufmann, 2011, pp. 305-349.

[28] T. Hastie, R. Tibshirani and J. Friedman, The Elements of Statistical Learning: Data Mining, Inference, and Prediction, Stanford, CA: Springer, 2008.

[29] T. Tan, Z. Yang, F. Chang and K. Zhao, "Prediction of the FirstWeighting from the Working Face Roof in a Coal Mine Based on a GA-BP Neural Network," *Appl. Sci.,* 2019.

[30] M. Millidere, H. B. Kurt, H. Ballı and Ö. Uğur, "Kalman Based Neural Network Analysis with Resampling Methods for Longitudinal Aerodynamic Coefficient Estimation," in *AIAA Aviation Forum*, Virtual Event, 2020.

[31] D. E. Goldberg, Genetic Algorithms in Search, Optimization and Machine Learning, Boston, MA: Addison Wesley Longman Publishing Co., Inc., 1989.

[32] S. N. Sivanandam and S. N. Deepa, Introduction to Genetic Algorithms, Berlin, Heidelberg: Springer, 2008.

[33] A. Chipperfield, P. Fleming, H. Pohlheim and C. Fonseca, "Genetic Algorithm Toolbox User's Guide," University of Sheffield, Sheffield, 2007.

[34] S. D. Sudhoff, "Genetic Optimization System Engineering Tool (GOSET) For Use with MATLAB," Purdue University, Purdue, 2007.

[35] L. He, W. Qian, T. Zhao and Q. Wang, "Multi-Fidelity Aerodynamic Data Fusion with a Deep Neural Network Modeling Method," *Entropy,* 2020.

[36] V. Klein and E. A. Morelli, Aircraft System Identification: Theory and Practices, Reston, Va: AIAA Education Series, 2006.

[37] H. Jiangtao, G. Zhenghonh, Z. Zhu and Z. Ke, "An improved adaptive sampling and experiment design method for aerodynamic optimization," *Chinese Journal of Aeronautics,* 2015.

[38] L. Nguyen, M. Ogburn, W. P. Gilbert, K. S. Kibler, P. W. Brown and P. L. Deal, "Simulator Study of Stall/PostStall Characteristics of a Fighter Airplane with Relaxed Longitudinal Static Stability," NASA Technical Paper 1538, Hampton, VA, 1979.

[39] William2002730. [Online]. Available: hangar.openvsp.org/vspfiles/343. [Accessed 05 06 2020].

[40] M. Fox and D. Forrest, "Supersonic Aerodynamic Characteristics of an Advanced F-16 Derivative Aircraft Configuration," NASA Technical Paper 3355, 1993.

[41] K. Abhary, S. D. Dao and R. Marian, "Maximising Performance of Genetic Algorithm Solver in Matlab," *Engineering Letters,* 2016.

[42] B. Peerlings, "A review of aerodynamics flow models, solution methods and solvers and their applicability to aircraft conceptual design," Delft University of Technology, Delft, 2018.

[43] K. Buzdiak, "Aerodyanmic Anaylsis with Athena Vortex Lattice (AVL)," Hamburg University of Applied Sciences, Hamburg, 2015.

[44] H. Y. M. Drela, "AVl User Primer - AVL 3.36," Massachusetts Institute of Technology, 2017.

[45] J. D. Anderson, Fundamentals of Aerodynamics, New York: McGraw-Hill, 2001.

[46] R. D. M. D. N. Raghunath K, "Uncertainty propagation for a subsonic aircraft in," in *In 15th AIAA/ISSMO Multidisciplinary Analysis and Optimization Conference*, Atlanta, 2014.

Appendix

A. Geometric Details

The geometric properties that are primarily required are the basic dimensions specified in the publicly available Saab 340B's manuals. Although, the basic geometric measurements are not sufficient for estimation of the aerodynamic properties using ESDU. Calculations of each aerodynamic derivative requires geometric parameters, specified in respective ESDU document, which are not commonly available in aircraft manuals. These parameters are thus obtained by physical measurements from the aircraft's scaled down diagrams. A few of the basic geometric parameters of the aircraft are listed below.

Table A.1 Wing Geometry

#	Description	Notation	Value	Unit
1	Span	b_w	21.44	m
2	Gross Wing Area	S_w	41.8	m^2
3	Exposed Wing Area	S_{we}	35.0	m^2
4	Aspect Ratio	A_w	11	m
5	Root Chord	c_{r_w}	2.67	m
6	Tip Chord	c_{t_w}	1.06	m
7	Mean Aerodynamic Chord	$\bar{c}_w$	2.08	m
8	Full Surface Length	l_w	10.799	m
9	Centreline Chord	c_{0_w}	2.83	m
10	Taper Ratio	λ_w	10.375	–
11	Twist Angle	δ_w	-2	°
12	Dihedral Angle	Γ_w	7	°

Table A.2 Vertical Tail (Fin) Geometry

#	Description	Notation	Value	Unit
1	Span	b_{vt}	3.7338	m
2	Gross Area	S_{vt}	7.043	m^2
3	Aspect Ratio	A_{vt}	3.6	–
4	Taper Ratio	λ_{vt}	0.37	–
5	Root Chord	$c_{r_{vt}}$	3.55	m
6	Tip Chord	$c_{t_{vt}}$	1.31	m

Table A.3 Horizontal Tail Geometry

#	Description	Notation	Value	Unit
1	Span	b_{ht}	9.25	m
2	Gross Area	S_{ht}	14.57	m^2
3	Aspect Ratio	A_{ht}	5.87	m
4	Root Chord	$c_{r_{ht}}$	1.97	m
5	Tip Chord	$c_{t_{ht}}$	1.03	m
6	Full Surface Length	l_{ht}	4.79	m
7	Centreline Chord	$c_{0_{ht}}$	2.14	m
8	Taper Ratio	λ_{ht}	0.478	–
9	Dihedral Angle	Γ_{ht}	15	°
10	Mean Aerodynamic Chord	$\bar{c}_{ht}$	?	m

Table A.4 Fuselage Geometry

#	Description	Notation	Value	Unit
1	Maximum Diameter	D_f	2.31	m
2	Forebody Length	l_{f_f}	2.62	m
3	Afterbody Length	l_{a_f}	5.38	m
4	Surface Area	S_f	254.52	m^2
5	Total Length	l_f	19.65	m
6	Midbody Length	l_{m_f}	11.65	m
7	Side Elevation Area	S_{S_f}	36.62	m^2

a. Mass Properties

The empty fuselage with no crew or passengers, has a mass of 4328 kg, and the empty wing has a mass of 1766 kg. The moments of inertia about their own cg are:

Table B.1. Inertia of fixed structures

Component	I_{xx} (kg. m^2)	I_{yy} (kg. m^2)	I_{zz} (kg. m^2)	I_{xz} (kg. m^2)
Wings	5062	63217	63217	0
Empty Fuselage	55710	2002	32574	349

Table B.2 Mass and CG location of undercarriage

Component	Mass (kg)	CG (Config. - UP)			CG (Config. - DWN)		
		x (m)	y (m)	z (m)	x (m)	y (m)	z (m)
Nose UC	116	3.937	0	1.0414	4.3942	0	1.7272
Main UC (left)	167	10.795	6.7056	1.1176	11.6332	6.7056	1.778
Main UC (right)	167	10.795	−6.7056	1.1176	11.6332	−6.7056	1.778

Table B.3. Mass and CG location of fixed structures

Component	Mass (kg)	CG		
		x (m)	y (m)	z (m)
Horizontal Tail (left)	117	19.812	1.524	−0.508
Horizontal Tail (right)	117	19.812	−1.524	−0.508
Vertical Tail	218	20.9804	0	−1.9812
Engine (left)	367	9.4234	3.3528	0.2388
Engine (right)	367	9.4234	−3.3528	0.2388
Propeller (left)	92	8.1788	3.3528	0.2388
Propeller (right)	92	8.1788	−3.3528	0.2388
Empty Fuselage	4328	10.1854	0	0
Wings	1766	11.27	0	0.5156

B. Input Files for AVL and DATCOM

1) AVL

```
Saab340B
0.2                 !  Mach
0    0    0.0      !  iYsym  iZsym  Zsym
41.8 2.08  21.24     !  Sref[m^2]   Cref[m]   Bref[m]   reference area, chord, span
8.45  0.0   0.0      !  Xref   Yref   Zref   moment reference location (arb.)
#==============================================================
SURFACE
Wing
12  1.0  26  1.0   ! Nchord   Cspace   Nspan  Sspace
# reflect image wing about y=0 plane
YDUPLICATE
    0.00000
# twist angle bias for whole surface
ANGLE
```

```
    2.00000

# x,y,z bias for whole surface
TRANSLATE
   7.88000     0.0     0.0
#---------------section 1-------------------------------------------------
#    Xle         Yle         Zle         chord       angle
SECTION
     0        1.12        0.0           2.7        0.000
AFILE
SaabAirfoil.dat
#Cname   Cgain  Xhinge  HingeVec       SgnDup
CONTROL
flap     1.0    0.802    0.0 1.0 0.0     1.1
#--------section2----------------------
SECTION
   0.565       7.364    0.675          1.7        0.000
AFILE
SaabAirfoil.dat
CONTROL
flap     1.0    0.802    0.0 1.0 0.0     1.0
CONTROL
aileron  1.0    0.65     0.0 1.0 0.0    -1.0
#--------section3----------------------
SECTION
   0.830       10.305        0.990       1.210        0.000
AFILE
SaabAirfoil.dat
CONTROL
aileron  1.0    0.65     0.0 1.0 0.0    -1.0
#--------section4----------------------
SECTION
   1.109       10.647        1.035       0.91        0.000
AFILE
SaabAirfoil.dat
SURFACE
H-Stab
8  1.0  15  1  !  Nchord   Cspace
# reflect image wing about y=0 plane
YDUPLICATE
    0.00000
# twist angle bias for whole surface
ANGLE
    0.00000
# x,y,z bias for whole surface
TRANSLATE
  16.54     0.0     1.260000
SCALE
 1.000  1.0  1.0
#----------------------section1-----------------------------------------
#    Xle         Yle         Zle         chord       angle
SECTION
     0          0.0        0.0          1.990        0
NACA
0012
```

```
CONTROL
elevator  1.0    0.35    0.0 1.0 0.0     1.0
#--------------section2---------------
SECTION
  0.570         3.150        0.870         1.016       0
NACA
0012
CONTROL
elevator  1.0    0.35    0.0 1.0 0.0     1.0
#--------------section3---------------
SECTION
  0.622         3.600        0.935         0.950      0
NACA
0012
SURFACE
Rudder
8  1.0  14  -1.1  ! Nchord   Cspace
#
# x,y,z bias for whole surface
TRANSLATE
  12.06     0.00000     1.80
#---------------section1-------------------------------------------------
#    Xle         Yle         Zle         chord       angle
SECTION
    0.0         0.0         0.0         7.56        0.000
CONTROL
rudder    1.0    0.80    0.0 0.0 1.0
#--------------section2---------------
SECTION
  4.156         0.0         0.606         3.30       0.000
CONTROL
rudder    1.0    0.45    0.0 0.0 1.0
#--------------section3----------------
SECTION
  7.720        0.0         3.370         1.715      0.000
CONTROL
rudder    1.0    0.45    0.0 0.0 1.0
#=============================================================
```

2) DATCOM clean

```
DIM M
 $FLTCON NMACH = 1.0, MACH(1)=0.20, NALPHA = 20.0,
   ALSCHD(1)=-9.0,-7.0,-5.0,-4.0,-2.0,-1.0,0.0,
   1.0,2.0,4.0,5.0,7.0,9.0,10.0,11.0,12.0,13.0,
   14.0,15.0,17.0,
        ALT(1)=0.0, STMACH=0.8, TSMACH=1.0$
 $OPTINS SREF=41.8, CBARR=2.08, BLREF=21.44$
 $SYNTHS XCG=8.454, ZCG=0.0, XW=7.674, ZW=0.322, ALIW=2.0,
   XH=16.3, ZH=1.269, ALIH=-0.478, XV=13.933,ZV=-0.217, VERTUP=.TRUE.$
 $BODY NX = 11.0,
   X(1)=0.0,0.120,0.6593,1.107,2.263,3.363,13.589,15.720,17.618,18.924,19.615,
   R(1)=0.0,0.206,0.538,2.249,3.43,3.658,3.658,3.221,2.01,1.03,0.0,
   S(1)=0.0,0.134,0.91,1.61,3.75, 4.261, 4.261,3.304,1.29,0.34,0.0,
   P(1)=0.0,1.301,3.463,4.77,6.91,7.317,7.317,6.490,4.059,2.071,0.0,
   ZU(1)=0.0,0.224,0.615,0.844,1.708,1.799,1.799,1.745,1.513, 1.282,0.0,
   ZL(1)=0.0,-0.1839,-0.354,-0.409,-0.495,-0.530,-0.530,-0.209,0.301,0.649,0.0,
```

```
  METHOD=2.0$
 $WGPLNF CHRDTP=1.06,  SSPNE=9.497, SSPN=10.615,
  CHRDR=2.67, SAVSI=5.2, CHSTAT=0.25, DHDADI=7.0, TWISTA=-2.0,
  TYPE=1.0$
 $HTPLNF CHRDTP=1.03, SSPNE=3.971, SSPN=4.385, CHRDR=1.97, SAVSI=10.35,
  CHSTAT=0.25, DHDADI = 15, TWISTA=0.478, TYPE=1.0$                    ** ERROR **  0*A  0*B  0*C
0*D  0*E  1*F
 $VTPLNF CHRDTP=1.31, SSPNE=3.884, SSPN=5.173, CHRDR=3.55, SAVSI=37.26,
  CHSTAT=0.25,  TWISTA=0.0, TYPE=1.0$
NACA-W-6-63-215
NACA-H-4-0012
NACA-V-4-0010
CASEID Saab340
DAMP
SAVE
NEXT CASE
```

3) DATCOM Flap

```
DIM M
 $FLTCON NMACH = 1.0, MACH(1)=0.20, NALPHA = 20.0,
  ALSCHD(1)=-9.0,-7.0,-5.0,-4.0,-2.0,-1.0,0.0,
  1.0,2.0,4.0,5.0,7.0,9.0,10.0,11.0,12.0,13.0,
  14.0,15.0,17.0,
      ALT(1)=0.0, STMACH=0.8, TSMACH=1.0$
 $OPTINS SREF=41.8, CBARR=2.08, BLREF=21.44$
 $SYNTHS XCG=8.454, ZCG=0.0, XW=7.674, ZW=0.322, ALIW=2.0,
  XH=16.3, ZH=1.269, ALIH=-0.478, XV=13.933,ZV=-0.217, VERTUP=.TRUE.$
 $BODY NX = 11.0,
  X(1)=0.0,0.120,0.6593,1.107,2.263,3.363,13.589,15.720,17.618,18.924,19.615,
  R(1)=0.0,0.206,0.538,2.249,3.43,3.658,3.658,3.221,2.01,1.03,0.0,
  S(1)=0.0,0.134,0.91,1.61,3.75, 4.261, 4.261,3.304,1.29,0.34,0.0,
  P(1)=0.0,1.301,3.463,4.77,6.91,7.317,7.317,6.490,4.059,2.071,0.0,
  ZU(1)=0.0,0.224,0.615,0.844,1.708,1.799,1.799,1.745,1.513, 1.282,0.0,
  ZL(1)=0.0,-0.1839,-0.354,-0.409,-0.495,-0.530,-0.530,-0.209,0.301,0.649,0.0,
  METHOD=2.0$
 $WGPLNF CHRDTP=1.06,  SSPNE=9.497, SSPN=10.615,
  CHRDR=2.67, SAVSI=5.2, CHSTAT=0.25, DHDADI=7.0, TWISTA=-2.0,
  TYPE=1.0$
 $SYMFLP NDELTA=4.0, DELTA(1)=0.0,7.0,15.0, 20.0, PHETE=0.003132,
  PHETEP=0.002378, CHRDFI=0.536, CHRDFO=0.357, SPANFI=1.118, SPANFO=7.353$
 $VTPLNF CHRDTP=1.31, SSPNE=3.884, SSPN=5.173, CHRDR=3.55, SAVSI=37.26,
  CHSTAT=0.25,  TWISTA=0.0, TYPE=1.0$
NACA-W-6-63-215
NACA-V-4-0010
CASEID Saab340
DAMP
SAVE
NEXT CASE
```

4) DATCOM Elevator

```
DIM M
 $FLTCON NMACH = 1.0, MACH(1)=0.20, NALPHA = 20.0,
  ALSCHD(1)=-9.0,-7.0,-5.0,-4.0,-2.0,-1.0,0.0,
  1.0,2.0,4.0,5.0,7.0,9.0,10.0,11.0,12.0,13.0,
  14.0,15.0,17.0,
      ALT(1)=0.0, STMACH=0.8, TSMACH=1.0$
 $OPTINS SREF=41.8, CBARR=2.08, BLREF=21.44$
```

```
 $SYNTHS XCG=8.454, ZCG=0.0, XW=7.674, ZW=0.322, ALIW=2.0,
   XH=16.3, ZH=1.269, ALIH=-0.478, XV=13.933,ZV=-0.217, VERTUP=.TRUE.$
 $BODY NX = 11.0,
   X(1)=0.0,0.120,0.6593,1.107,2.263,3.363,13.589,15.720,17.618,18.924,19.615,
   R(1)=0.0,0.206,0.538,2.249,3.43,3.658,3.658,3.221,2.01,1.03,0.0,
   S(1)=0.0,0.134,0.91,1.61,3.75, 4.261, 4.261,3.304,1.29,0.34,0.0,
   P(1)=0.0,1.301,3.463,4.77,6.91,7.317,7.317,6.490,4.059,2.071,0.0,
   ZU(1)=0.0,0.224,0.615,0.844,1.708,1.799,1.799,1.745,1.513, 1.282,0.0,
   ZL(1)=0.0,-0.1839,-0.354,-0.409,-0.495,-0.530,-0.530,-0.209,0.301,0.649,0.0,
   METHOD=2.0$
 $WGPLNF CHRDTP=1.06,  SSPNE=9.497, SSPN=10.615,
   CHRDR=2.67, SAVSI=5.2, CHSTAT=0.25, DHDADI=7.0, TWISTA=-2.0,
   TYPE=1.0$
 $HTPLNF CHRDTP=1.03, SSPNE=3.971, SSPN=4.385, CHRDR=1.97, SAVSI=10.35,
   CHSTAT=0.25, DHDADI = 15, TWISTA=0.478, TYPE=1.0$                    ** ERROR **  0*A  0*B  0*C
0*D  0*E  1*F
 $SYMFLP NDELTA=7.0, DELTA(1)=-22.0,-10.0,-5.0,0.0,5.0,10.0,18.0,
   PHETE=0.003527, PHETEP=0.0033638, CHRDFI=0.7799, CHRDFO=0.4639, SPANFI=0.7478   ** ERROR **
0*A  0*B  0*C  0*D  0*E  1*F
   SPANFO=4.1143$
 $VTPLNF CHRDTP=1.31, SSPNE=3.884, SSPN=5.173, CHRDR=3.55, SAVSI=37.26,
   CHSTAT=0.25,  TWISTA=0.0, TYPE=1.0$
NACA-W-6-63-215
NACA-H-4-0012
NACA-V-4-0010
CASEID Saab340B
DAMP
SAVE
NEXT CASE
```

Aerodynamic analysis of Saab 340B aircraft with data fusion implementation

Sahin, Kadir

2024-01-04

Sahin K, Gomec F, Millidere M, Whidborne J. (2024) Aerodynamic analysis of Saab 340B aircraft with data fusion implementation. In: AIAA SCITECH 2024 Forum, 8-12 January 2024, Orlando, USA. Paper number AIAA 2024-2854

https://doi.org/10.2514/6.2024-2854